Meccanica (2017) 52:3661–3674
DOI 10.1007/s11012-017-0692-3

Duty cycle and directional jet effects of a plasma actuator on the flow control around a NACA0015 airfoil

Carlo A. Borghi · Andrea Cristofolini · Gabriele Neretti · Paolo Seri · Alessandro Rossetti · Alessandro Talamelli

Received: 6 August 2016 / Accepted: 10 May 2017 / Published online: 3 June 2017

Abstract This paper reports on the effects of a series of fluid-dynamic dielectric barrier discharge plasma actuators on a NACA0015 airfoil at high angle of attack. A set of jet actuators able to produce plasma jets with different directions (vectoring effect) and operated at different on/off duty cycle frequencies are used. The experiments are performed in a wind tunnel facility. The vectorized jet and the transient of the flow induced by unsteady duty cycle operation of each actuator are examined and the effectiveness of the actuator to recover stall condition in the range of Reynolds numbers between 1.0×10^5 and 5.0×10^5 (based on airfoil chord), is investigated. The actuator placed on the leading edge of the airfoil presents the most effective stall recovery. No significant effects can be observed for different orientations of the jet. An increase of the stall recovery is detected when the actuator is operated in unsteady operation mode. Moreover, the frequency of the on/off duty cycle that maximizes the stall recovery is found to be a function of the free stream velocity. This frequency seems to scale with the boundary layer thickness at the position of the actuator. A lift coefficient increase at low free stream velocities appears to linearly depend on the supply voltage.

Keywords Aerodynamics · Flow control · Plasma flow control · DBD discharges · Electro-hydro-dynamics · Plasma actuator

C. A. Borghi · A. Cristofolini · G. Neretti · P. Seri
Department of Electrical, Electronic and Information Engineering, University of Bologna, Viale Risorgimento 2, Bologna, Italy
e-mail: ca.borghi@unibo.it

A. Cristofolini
e-mail: andrea.cristofolini@unibo.it

G. Neretti
e-mail: gabriele.neretti@unibo.it

P. Seri
e-mail: paolo.seri2@unibo.it

A. Rossetti · A. Talamelli (✉)
Department of Industrial Engineering, University of Bologna, Via Fontanelle 40, Forlì, Italy
e-mail: alessandro.talamelli@unibo.it

A. Rossetti
e-mail: alessandro.rossetti@unibo.it

1 Introduction

In the last two decades flow control in fluid dynamics has attracted an increasing interest with an impressive development of technologies to realize it. Passive control techniques are still broadly used since they do not require external energy input. Nevertheless the interest on active control strategies has recently obtained a large attention since they operate in a selective way and only when it is effectively required.

Among different active techniques, plasma actuators, based on the electro hydro dynamic (EHD) interaction effect, have been extensively studied since

they are dynamically active, they do not present moving parts, and are characterized by short actuation times [1]. Moreover, they have a very low weight, can be easily constructed, and generate very low aerodynamic interferences when are not used. When activated, they can significantly modify the boundary layer development on body surfaces. For this reason they have been extensively studied for aeronautical applications to prevent flow separation by enhancing lift and reducing drag (see as a review Moreau [2] and Wang et al. [3]). More recently they have been used also to control friction drag by delaying transition [4, 5] or by oscillating the flow in the spanwise direction [6], and to control global instabilities of the flow (Moreau [2], Wang et al. [3], and Touchard [7]). Due to these characteristics the potential of plasma actuators, operating through the EHD interaction, has been extended to many other applications as, for instance, automotive and energy production (Vernet et al. [8], Greenblatt et al. [9]).

A great number of experimental and numerical works have been done in the last decade to both understand the basic physical phenomena involved in the interaction (see for instance, Borghi et al. [10, 11], Pons et al. [12], Opaits et al. [13, 14], Dawson and Little [15], Thomas et al. [16], Cristofolini et al. [17–19], Filoppimin et al. [20], Nishida [21], and Kotsonis et al. [22]), and evaluate aerodynamic effects on surfaces (Neretti [23], Moreau [2], Post [24], He [25], and Rizzetta [26]). A classical EHD plasma actuator induces a jet in the direction tangential to the surface of the actuator itself, similarly to a classic blowing technique (see the review by Bénard and Moreau [27]). These jets can modify the aerodynamic boundary layer, increasing momentum transfer to the flow, at least in the near-wall region above the surface. However, plasma aerodynamic actuators can be also used to generate a pulsating jet flowing in a direction different from the tangential one (Benard et al. [28], Amitay [29], Kim [30]). In this way, the actuator induces inside the boundary layer a flow similar to that produced by a synthetic jet, enhancing the dynamic response and lowering the weight of the whole actuating system. For this reason these type of actuators are called Plasma Synthetic Jet Actuators (PSJA). In the last years several investigations have dealt with PSJA built by means of DBDs or Sliding Discharges in annular and linear configurations (Santhanakrishnana and Jacob [31], Bénard et al. [32], Bolitho and Jacob [33], Matsuno et al. [34], Sosa et al. [35], Seney et al. [36], Moreau [37], Neretti et al. [38]). In a previous work (Neretti et al. [39]), a vectorized plasma jet DBD actuator, capable to induce a jet in a desired direction, has been experimentally investigated. The vectoring effect is obtained by varying both applied voltages and electrical connections of the electrodes. In this cited work the actuator has been qualitatively and quantitatively characterized showing a proportional relation between the jet deflection angle and the applied voltage. Moreover, a linear relation between the maximum speed in the jet direction and the voltage has been found.

In the present work a set of vectorized plasma jet actuator arrays is mounted on the surface of a NACA0015 airfoil. An experimental investigation in a subsonic wind tunnel facility has been carried out. Free stream velocities of the flow, ranging between 5 and 23 m/s, corresponding to a Reynolds number between 1.0×10^5 and 4.6×10^5, are considered. In order to reach the complete stall in all flow conditions, angles of attack up to 26° are set up. The actuators array is made by a series of DBD actuators mounted along the airfoil surface. Each actuator unit can be operated alone to determine the effect of the position on the control strategy. The DBD actuation is used in the continuous operation and in the unsteady duty cycle mode. The unsteady actuation is obtained by an on/off periodic duty cycle (50% of the period on and 50% off) that causes a sequence of transients in the jet flow. Duty cycle frequencies between 5 and 200 Hz are used. Jet position, jet orientation, duty cycle frequency and supplying voltage are investigated. Their effects on the stall recovery are determined. This combined parametric study is performed in order to define an optimized strategy for the effective control of the DBD actuation.

2 Experimental set-up

The experiments are carried out in the laboratory of the University of Bologna. The wind tunnel is an open-return type with a 1.9 m long rectangular test section 0.90×0.60 m^2. The flow is provided by a 39 kW axial-fan, capable to set and keep a stable velocity in the test section from 1 to 55 m/s. A good quality flow in terms of homogeneity and free stream turbulence (0.3% at 20 m/s) is obtained by means of a

series of screens and a honeycomb mounted in the settling chamber.

To perform the analysis a standard NACA0015 airfoil with a chord of 0.31 m and a span of 0.33 m (see Fig. 1a) is mounted in the test section. To minimize three dimensional effects, two circular Plexiglass plates with a diameter of 0.38 m are mounted at the tips of the wing.

The actuator electrodes, used to generate the discharge, are positioned on the wing surface along the span-wise direction (Fig. 1b). On the surface, small tufts are mounted in order to qualitatively show the extension of the separated region and to check the absence of significant 3D effects.

The reference speed in the test section is measured by means of a Prandtl probe positioned in the undisturbed region of the flow. The probe is connected with a Setra 239 pressure transducer with a full scale output of 2500 Pa, and an accuracy of $\pm 0.14\%$.

A six components DELTATECH balance, based on strain gauges technique, is used to measure the lift of the airfoil. In order to fix the angle of attack of the airfoil, a step-by-step phase VEXTA electric motor with a resolution of 0.024°/step is used. Experimental data are detected by means of a National Instrument NI-USB 6221 acquisition board, connected to a computer through a Labview program, which controls automatically the whole setup.

In Fig. 2 the schematic of two actuator units, which produces a vectorized jet, is shown. The actuators are similar to those used by Neretti et al. [39]. Two upper electrodes (Up 1 and Up 2) are placed at a distance of 15 mm. The electrodes are made of copper strips. They are 5 mm large (x-direction in Fig. 2), 300 mm wide (z-direction), and 0.04 mm thick (y-direction). The upper electrodes are separated from four lower electrodes (Low 1, Low 2, Low 3, and Low 4) by a dielectric slab. Lower electrodes are copper strips, 7 mm large, and with the same width and thickness of the upper ones. They are placed at a distance of 3 mm from each other. In x-direction each upper electrode is placed between two lower electrodes, and upper and lower electrodes are superimposed of 1 mm on both sides to reduce the electric tip effect over their edge. The dielectric slab is 0.43 mm thick and is constituted by a 250 μm thick Mylar sheet between two 90 μm thick Kapton layers.

At both sides of each electrode, from the electrode edge, a plasma region, blowing above the dielectric surface in the tangential direction and toward the adjacent upper electrode, is produced. From the interaction of the two tangential induced jets on the dielectric surface between two adjacent electrodes, an overall jet in a diagonal direction is produced. The angle of the jet axis is determined by the voltages applied to the electrodes. Therefore, in order to generate a single vectorized jet, two adjacent units are utilized. On the NACA0015 airfoil a set of 8 units have been placed. Hence, as shown in Fig. 3, 9 vectorized jets with an adjustable direction in 9 different positions on the airfoil surface can be generated. Actuator 5 is placed on the leading edge

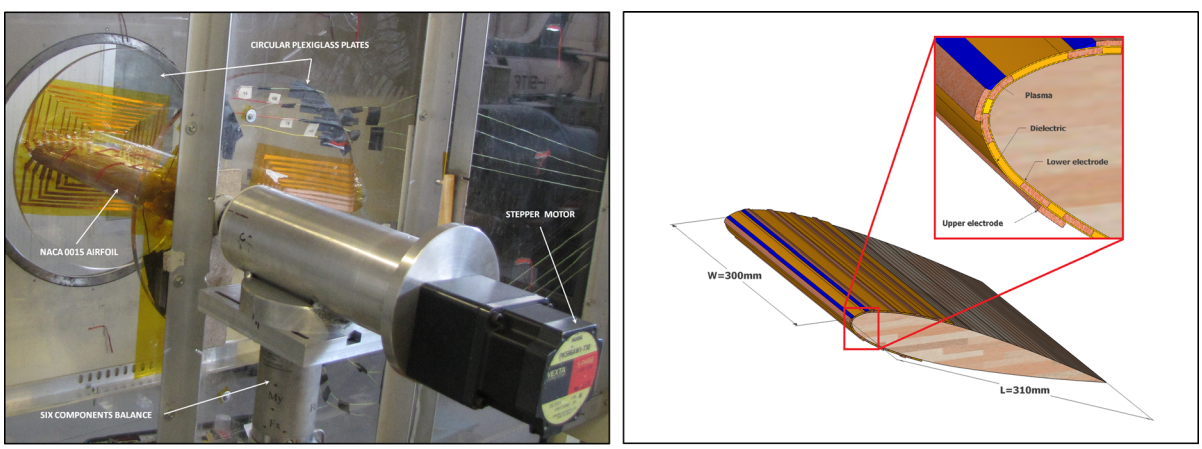

Fig. 1 **a** Snapshot of the set-up installed in the test-section, **b** schematic of the NACA0015 airfoil equipped with the DBD plasma actuators

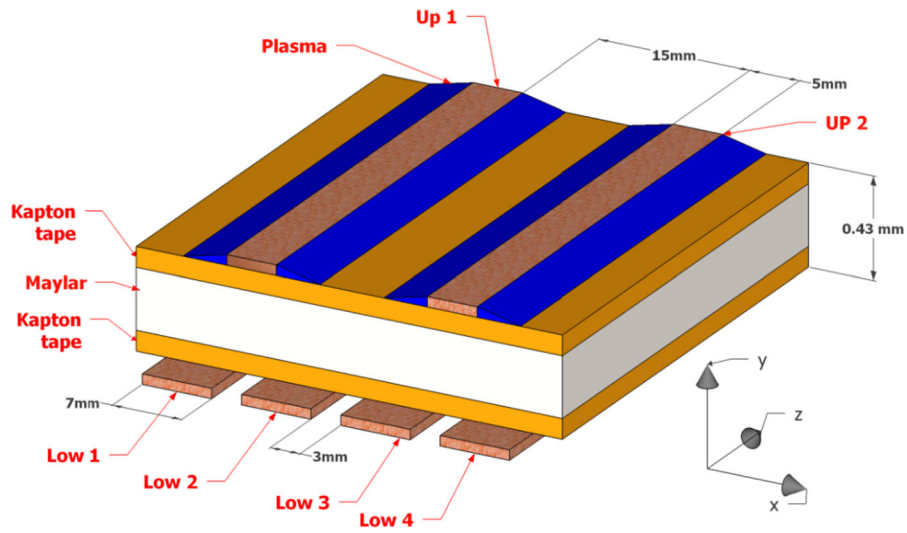

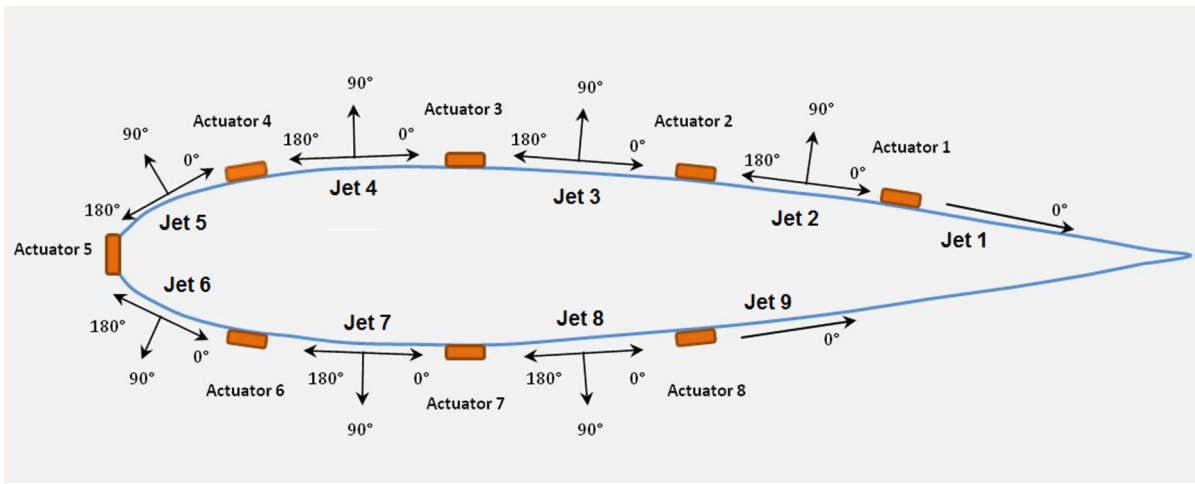

Fig. 2 Schematic of the electrode configuration

Fig. 3 Schematic describing the positions of actuators and jets over the airfoil

of the airfoil. An angle of 0° corresponds to a jet flowing tangentially along the free stream direction.

Schlieren diagnostic is used to display direction and morphology of the jets, i.e. electric wind, in still air. Images are obtained by a Z-type configuration setup. A tungsten halogen low voltage lamp equipped with a rear reflector generates the light source. The condenser of the optical system is a Schneider-Kreuznach Xenon 40 mm double-Gauss lens with a f/1.9 focal ratio. Two off-axis parabolic mirrors of a diameter of 138 mm and an f/3.5 focal ratio reflect the light beam. The light beam is oriented along the z-direction (Fig. 2). The knife-edge is parallel to the actuator surface (x-direction in Fig. 2) so that the Schlieren diagnostic can record density gradients perpendicular to the x–z plane (y-direction in Fig. 2). The images are detected by a PCO CCD camera, equipped by means of a super-video-graphics array (SVGA) resolution with a pixel size of $6 \times 6\ \mu m^2$. The peak quantum efficiency is 55% at a wavelength of 380 nm. Exposure time is fixed to 1 ms.

For the characterization of the electric wind in quiescent air velocity profiles are determined by means of a glass Pitot tube with an outer diameter of 1 mm while the direction is estimated by using Schlieren imaging. A step motor with a linear resolution of 0.03 mm moves the tube in the direction perpendicularly to the jet orientation. The Pitot tube is

connected to a DCAL401 Sursense ultra-low differential pressure sensor with a sensitivity of 32 mV/Pa. The velocity profiles are obtained by averaging 10 different measured values taken at the same condition. All measurements are filtered by using an analogic low pass filter with a cut-off frequency of 100 Hz. The measurement error is based on the standard deviation of measured data. All the results of measurements reported in this work are characterized by relative standard deviations well below 10%.

Actuators have been fed by a supply system constituted by a H-bridge brunch unit connected to a transformer cascade. This is done to increase the voltage to its operation value. In Fig. 4 a scheme of the power supply system is shown. The amplitude of the supply voltage ranges between 0 and 7.5 kV, and the frequency ranges between 1 and 25 kHz. The maximum average power is 200 W. The AC voltage supplied to the actuator is fixed at V_1. The variable voltage V_2 is obtained by means of a resistive voltage divider with the resistances R and R_0. The actuator impedance is much bigger than the resistance R_0, therefore the voltage V_2 is given by

$$V_2 = \frac{R_0}{R_0 + R} V_1 \tag{1}$$

The voltage V_2 is controlled by varying the value of R. Electric measurements confirmed that V_2 and V_1 are in phase. Voltages and current are detected by means of two Tektronix P6015A capacitive compensated high voltage probes, with a bandwidth up to 75 MHz, and a Tektronix TCP312 Hall current probe, with a bandwidth up to 100 MHz respectively. A Yokogawa DL1740 scope with a sample rate of 10^9 samples per second have been used to acquire the signals.

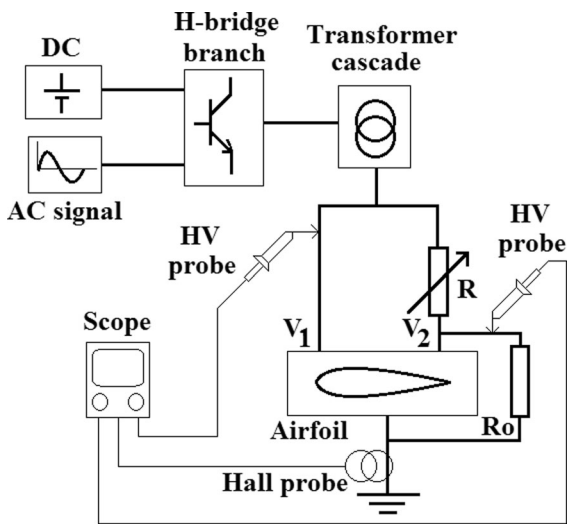

Fig. 4 Schematic of the electrical power supply system

3 Fluid dynamic characterization of vectorized jets

As shown in Fig. 2, each vectorized jet is induced by two consecutive actuator units. A full electric and fluid-dynamic characterization of a single vectorized jet in still air is reported by Neretti et al. [39]. Here, the jet actuator is used when operated both in the continuous and in the unsteady duty cycle mode. In the following, the electric wind generated by the vectorized jet in still air is presented. Velocity profiles, jet orientation and morphology have been assessed and described for jet directions of 0°, 45° and 90°. The vectoring effect on the jet is obtained by supplying the upper electrodes with sinusoidal voltages at different amplitudes. The voltage frequency has been set at 15 kHz for all tests. The electrical connections of the electrodes used in the present work are shown in Fig. 5.

Supply voltages, electrical connections and corresponding jet orientations for those investigated in this section are listed in Table 1.

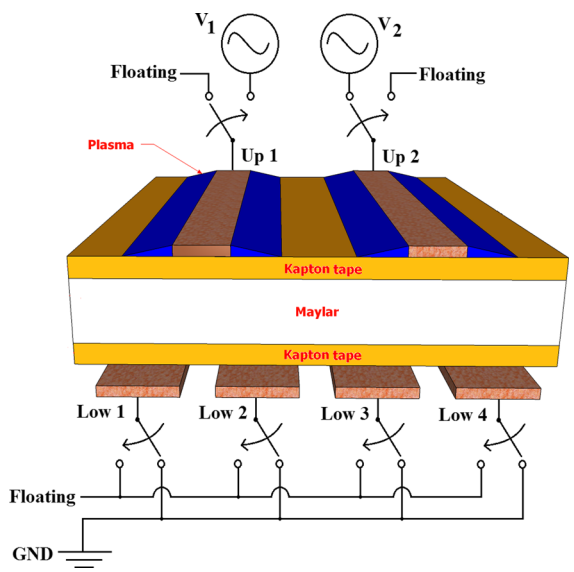

Fig. 5 Schematic of the electric connections of the electrodes

Average power delivered to electrodes has been evaluated as the average value of the product voltage-current feeding the discharge, within a sinusoidal voltage period. A tangential jet is obtained supplying electrodes with 38 W, a 45° jet with an average power of 57 W and a normal jet with 76 W.

Images of the electric wind produced by the actuators operated in different modes are shown in Figs. 6, 7 and 8. The continuous mode operation of the actuator is presented in Fig. 6. In the figure, the 'Scan distance' is the distance from the jet axis in the direction along which the Pitot tube has been moved. For all jet orientations the scan distance has been chosen approximately perpendicularly to the jet direction and is reported in the image.

The plot of Fig. 6a shows the velocity profile induced by a wall jet, i.e. with a deflection angle of 0°, measured 10 mm downstream of electrode Up 1 and perpendicularly to the jet direction (hence perpendicularly to actuator surface). The maximum speed measured on the axis of the jet is 4 m/s decreasing to 0 at about 2 mm far from the actuator surface. Velocity profiles of Fig. 6b, c refer to deflections of 45° and 90° respectively. For both orientations velocity profiles measured at 5, 10 and 20 mm from the jet starting point are displayed. The figures show that for different jet directions the behavior of the jet changes significantly. Despite higher average powers are supplied to the system to obtain an oriented jet, lower speeds are reached in comparison to those of the tangential jet configuration. On the other hand higher mass flow rates are present in the oriented jets.

Figure 7 shows images obtained with plasma actuators operating in unsteady mode. In this case the on/off switching of the actuator induces the formation of an unsteady vortex that develops along the jet direction and is finally conveyed by the mean flow induced by the plasma. This process occurs at each off/on switching event and hence once for each duty cycle period. Therefore, when the actuator is operated in a duty cycle mode, the flow regime is constituted by a sequence of unsteady jets. In this work the duty cycle has been fixed to 50% of the time period on, and 50% off.

In Fig. 7, Schlieren images of the 0° oriented jet (tangential jet) in the unsteady operation mode (Fig. 7a–d) and in the steady regime (Fig. 7e) for comparison are reported. The images have been acquired after 1 s from the start of the duty cycle operation. Exposure time has been set to 1 ms. The figure shows that the plasma actuator triggers the instability of the shear layer generating the roll-up of vortices. The frequency of the vortex generation is therefore the same of the actuation duty cycle frequency. When the duty cycle frequency is low, the dimensions of the eddies are large and they affect a large portion of the fluid near the actuator (compare the images of Fig. 7). By increasing the duty cycle frequency (Fig. 7c, d) the induced vortices progressively reduce their dimensions and propagate closer to the wall. At high frequencies, as in the steady operation, the jet follows the natural transition and remains confined close to the wall.

In Fig. 8 Schlieren images of the jet at 90° operated in the duty cycle mode at frequencies between 25 and 200 Hz and in the steady state mode are reported. In this case modifications occurring at different frequencies are not observed. Both jet width and vortex spreading appear to be similar.

4 Aerodynamic effects of the vectorized jet actuator on the NACA0015 airfoil

In this section the effects of the actuators on the aerodynamic forces generated on a NACA0015 airfoil are presented. Results obtained by using jets with different directions (0°, 45°, 90°, 135°, and 180°) are described. A free stream velocity of 11 m/s ($Re = 220\,000$) and an angle of attack of 19° are used for the tests. This corresponds to a condition for which a complete stall of the airfoil is obtained when the plasma

Table 1 Jet orientations dependence to electrical connections

Jet orientation (°)	Up 1	Up 2	Low 1	Low 2	Low 3	Low 4
0	6 kVp	Floating	Floating	Ground	Floating	Floating
45	6 kVp	4.2 kVp	Floating	Ground	Ground	Floating
90	6 kVp	6 kVp	Floating	Ground	Ground	Floating

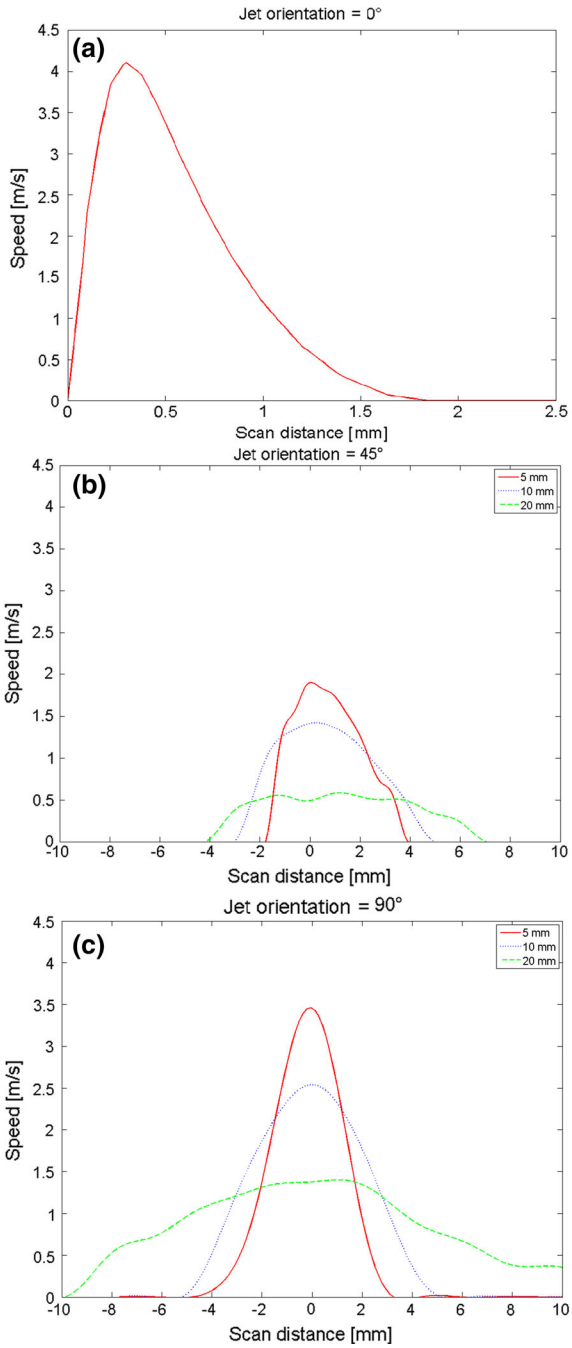

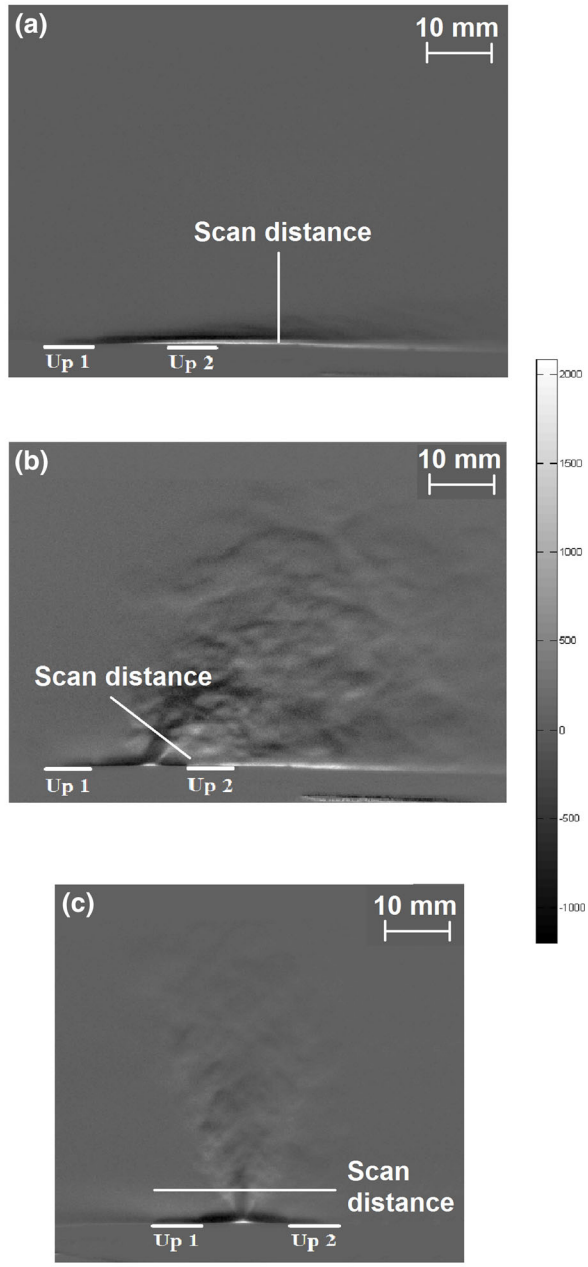

Fig. 6 Velocity profiles (*left*) and Schlieren images (*right*) for the jet orientations of 0° (**a**), 45° (**b**) and 90° (**c**). The velocity profile of the tangential jet (**a**) is taken at 10 mm from the upper high voltage electrode. For 45° (**b**) and 90° (**c**) jets, the profiles are taken at 5, 10 and 20 mm along the jet direction (measured from the jet starting point)

actuation is not active. Eight actuator units are placed on the airfoil resulting in nine induced jets at different positions (see Fig. 3). In the present investigation a couple of two adjacent actuator units is operated separately with the other actuators off. A preliminary analysis shows that jet 1, 2, 3, 7, 8, and 9 present a negligible effect on the stall recovery mechanism. For this reason, in the following, they will not be included

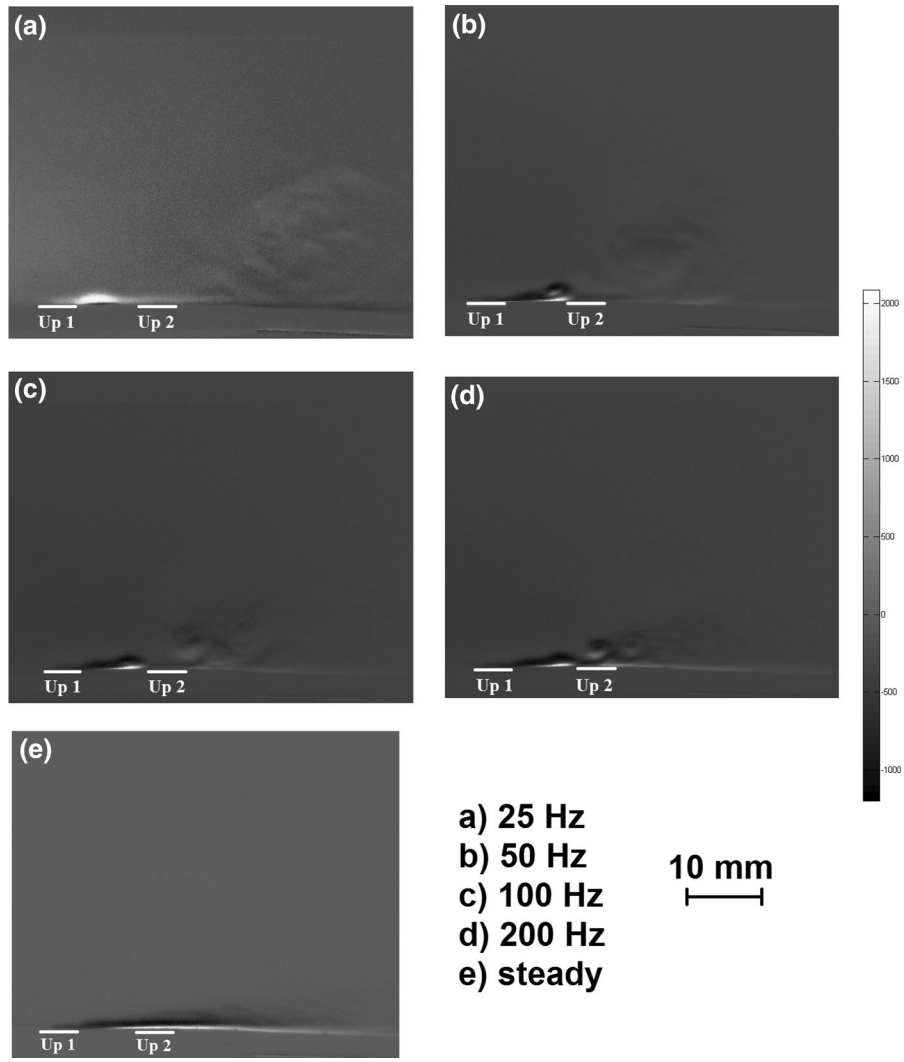

Fig. 7 Schlieren images for a jet orientation of 0° (tangential jet) at different actuation frequencies: **a** 25 Hz, **b** 50 Hz, **c** 100 Hz, **d** 200 Hz, **e** Steady

in the analysis. In Fig. 9a the effects induced by Jets 4, 5, and 6 on the stall recovery, as a function of jet orientation, are shown. The actuators are operated in the continuous mode. The figure shows the stall recovery, $C_{L\text{-recovery}}$ [%], calculated as the percentage ratio between lift coefficient measured by using the plasma actuation at 19° and the maximum C_L without plasma actuation.

In Fig. 9 the black horizontal line (baseline) represents the actual C_L obtained at an angle of attack of 19°, without plasma actuation (please note that it is 64% of the maximum C_L). According to this definition a C_L recovery of 100% corresponds to a complete recovery of the stall condition. For all cases, except for Jet 5 at 90°, when actuators are operated in the continuous mode, the dependence of the recovery on the orientation of jets seems to be rather weak. At 90° the recovery drops significantly. This behavior is probably associated to a separation of the boundary layer. The lack of a velocity diagnostic does not allow us to explain the rise at larger orientations, viz. 135° and 180°, which can be the object of a future experimental campaign.

The effects on the stall recovery of Jets 4, 5 and 6 with the duty cycle operation at a frequency of 25 Hz are shown in Fig. 9b. The stall recovery appears to be much more effective than the one obtained by the continuous operation. In this case the effect of the jet depends on its position on the airfoil surface. The contribution of Jet 4 to the stall recovery is negligible

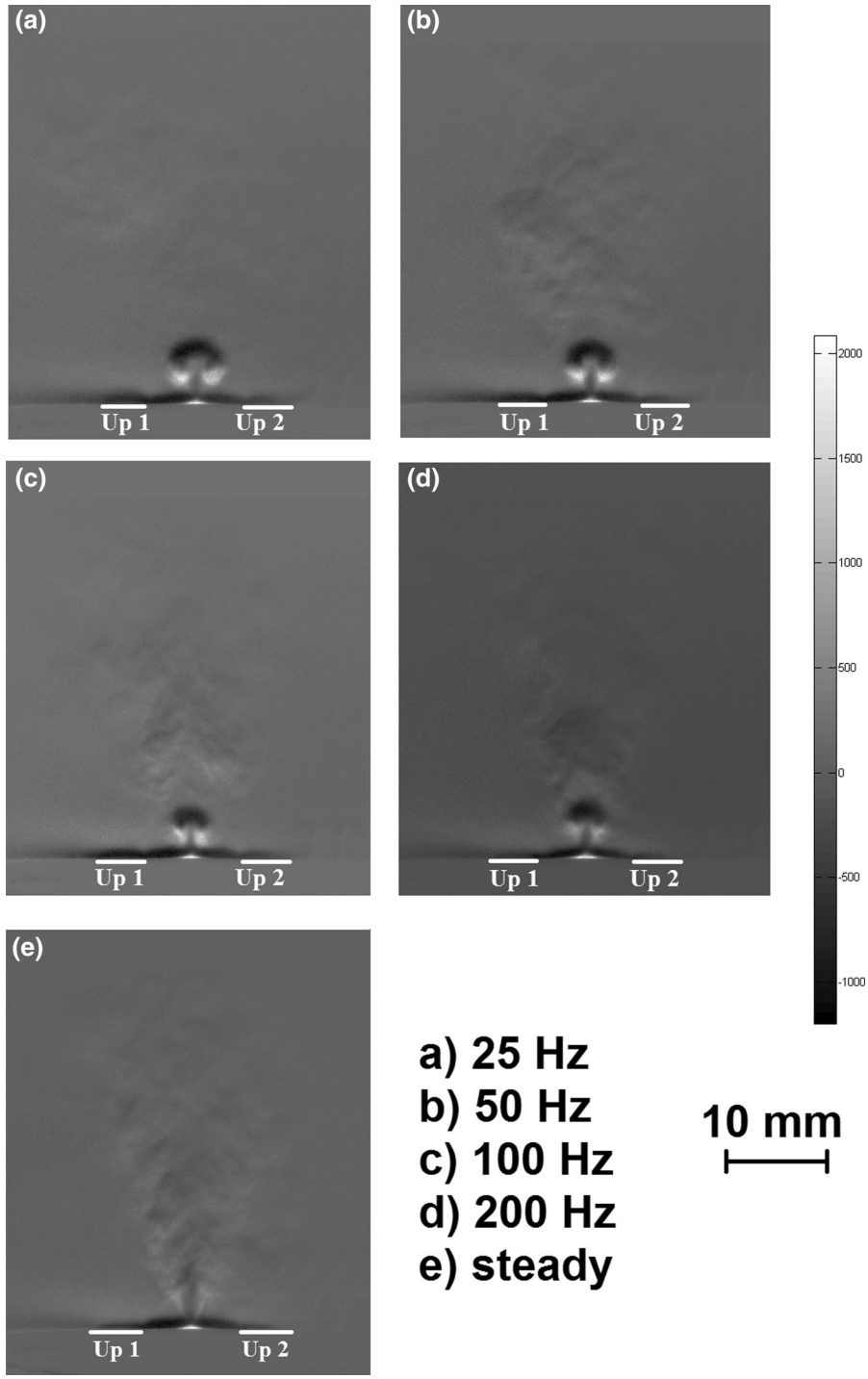

Fig. 8 Schlieren images for a jet orientation of 90° at different duty cycle frequencies: **a** 25 Hz, **b** 50 Hz, **c** 100 Hz, **d** 200 Hz, **e** Steady

for any jet orientation. This actuator is inside the aerodynamic wake and is too far downstream from the separation point to promote reattachment. Jet 5 is located just above the leading edge and is very close to the location of minimum pressure coefficient. It is placed before the separation point and promotes a nearly complete stall recovery for orientations smaller than 90°.

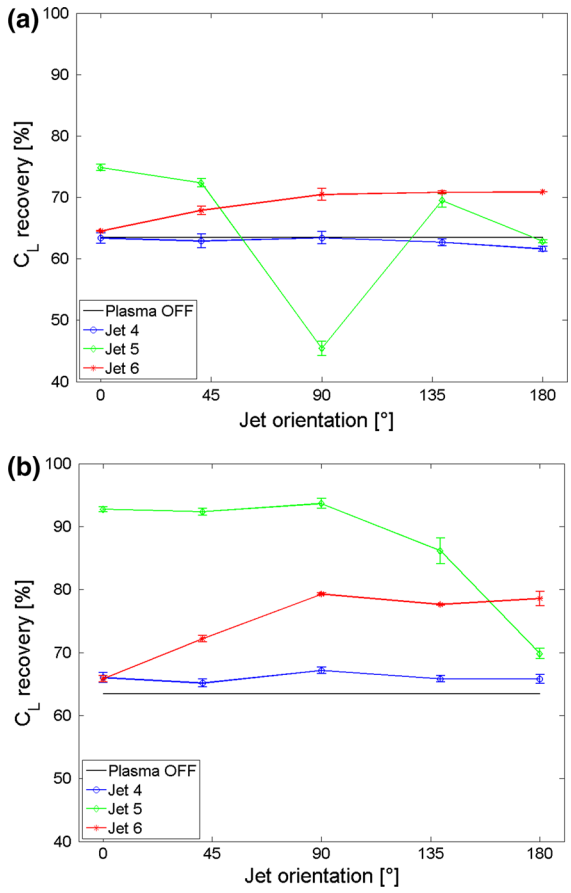

Fig. 9 Stall recovery in percentage for Jet 4, 5, and 6 with a free stream velocity of 11 m/s and angle of attack of 19°. Continuous plasma actuation (**a**) and duty cycle operation with a frequency of 25 Hz (**b**)

Jet 6 is located below the leading edge probably close to the front stagnation point. It produces a maximum stall recovery of 80% when it is oriented against the mean flow. This means for directions ranging between 90° and 180° (see Fig. 3). When Jet 6 is oriented backwards, thus toward the main flow direction, a stall recovery is still present but it appears to be strongly reduced. It is worth noticing that in any case, Jet 4, 5, and 6 always promote a lift recovery independently of their orientation. These results suggest that the stall recovery mechanism operated by the plasma actuators is mostly related to an energy deposition phenomenon, instead of a simple increment of the velocity in the boundary in the downstream direction [40–42]. Similar results have been obtained by other authors using mechanical devices [43, 44].

In order to evaluate the effect of the on/off duty cycle frequency, Jet 5 has been operated at different frequencies. The stall recovery, as a function of the duty cycle frequency, is reported in Fig. 10a, b. In order to highlight the effect of the actuation, tests have been performed at an angle of attack of 26°, with free stream velocities of 9 and 19 m/s. In the tests the jet direction is kept at 0°. It must be pointed out that this angle of attack leads to a deep stall condition for all free stream velocities investigated.

Figure 10 allows to identify an "optimal" frequency f_{opt}, at which the stall recovery is at maximum. The behavior of the stall recovery as a function of the on/off frequency is similar for all free stream velocities investigated. An initial steep increase of the lift coefficient is observed at frequencies of the order of 10–20 and 20–40 Hz for free stream velocity of 9 and 19 m/s respectively. Thereafter, when increasing the frequency of the duty cycle, the recovery decreases.

Figure 10 shows that, for both speeds, at frequencies larger than the optimal one, the decrement of the stall recovery with increasing the duty cycle frequency, is modest. Nevertheless, an optimal duty cycle frequency f_{opt}, at which the recovery is maximal, corresponding to a maximal response of the flow to the plasma actuation, can still be defined.

In Fig. 11 optimal duty cycle frequencies obtained for different values between 5 and 23 m/s of free stream velocity V are plotted. In order to find an analytical expression, a least squared fitting was applied to the obtained data. As a first attempt both linear and power laws have been used and the following expressions have been obtained:

$$f_{opt} = 2.9V - 10.1 \tag{2}$$

$$f_{opt} = 0.6V^{1.47} \tag{3}$$

Even though the difference is not very large, it is clear that a power law, with an exponent very close to 1.5, shows a better approximation. In an attempt to find a possible scaling for the optimal frequency, a non-dimensional frequency, i.e. Strouhal number, can be defined. In this context, several characteristics length can be chosen. A first natural choice is the chord length, L. However, following the experimental results, another good candidate could be the boundary layer thickness δ, which for laminar boundary layers is proportional to $V^{-1/2}$ [45]. This comes from the dependence of δ, in a laminar boundary layer, on the

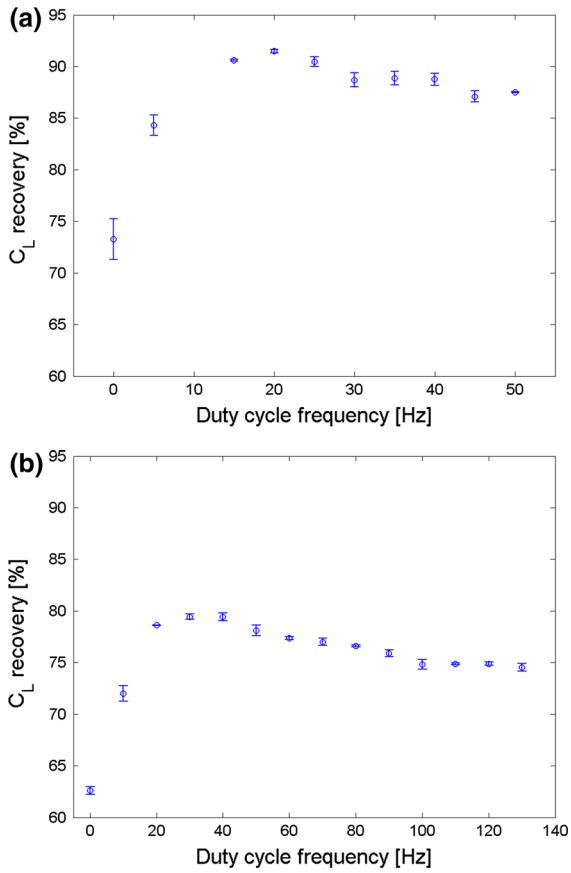

Fig. 10 Stall recovery in percentage obtained by using the jet 5 at 0° with an angle of attack of 26° and by using different duty cycle frequencies. Free stream velocity equal to 9 m/s (**a**) and 19 m/s (**b**)

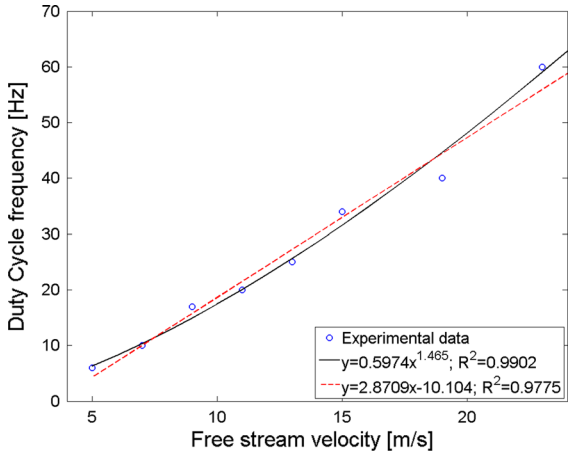

Fig. 11 Duty cycle frequency that optimizes the C_L recovery as a function of the free stream velocity. Data obtained by Jet 5 with a 0° orientation

inverse of the square root of the Reynolds number and, thus, on the inverse of the square root of the free stream velocity. By assuming $L_c = \delta$, and $\delta = C_1 V^{-1/2,}$ where C_1 is a coefficient, which depends on the actual laminar boundary layer evolution on the airfoil, and considering the experimentally observed optimal frequency, the Strouhal number is given by

$$St = \frac{fL_c}{V} = \frac{f_{opt}\delta}{V} = C1\frac{f_{opt}}{V^{1.5}} \quad (4)$$

It must be pointed out that the set-up does not allow us to measure the actual boundary layer thickness so the exact value of C1 cannot be evaluated. To remove this dependency the Strouhal number is normalized in comparison to its average value. Figure 12a shows the comparison between the normalized Strouhal number (St_L) calculated using the chord length of the airfoil as characteristic length, and the normalized Strouhal number (St_δ) evaluated using Eq. 4, for Jet 5 with a jet orientation of 0°. In Fig. 12b the same comparison is shown for Jet 5 with a jet orientation of 45°.

In both figures, St_δ shows a nearly constant behavior over the range of free stream velocities investigated. This indicates that the duty cycle frequency must be modified depending on the free-stream speed and must scale with the boundary layer thickness. It shall be pointed out that these results are obtained in the tests performed in the wind tunnel with free stream speeds compatible with the presence of a laminar boundary layer evaluated in the position of the actuator. A completely different scenario may apply in the presence of a turbulent boundary layer.

In Fig. 13, the percentage lift recovery of Jet 5 at the optimal frequency as a function of the free stream velocity for different jet orientations is shown. As previously observed the jet orientation does not sensibly affect the stall recovery. The main differences are detected at low speeds, where the jet at 0° produces the largest recovery. However, this difference decreases as the free stream velocity increases.

The lift recovery in a deep stall regime depends on the voltage supplying the actuator. In order to investigate this, a set of tests with different supply voltages at an angle of attack of 26° and with free stream velocities ranging from 9 to 19 m/s, is carried out. Jet 5 is operated with a duty cycle frequency of 20 Hz and an orientation of 0°. The percentage stall recovery obtained is plotted in Fig. 14. At a given free stream velocity the stall recovery linearly depends on

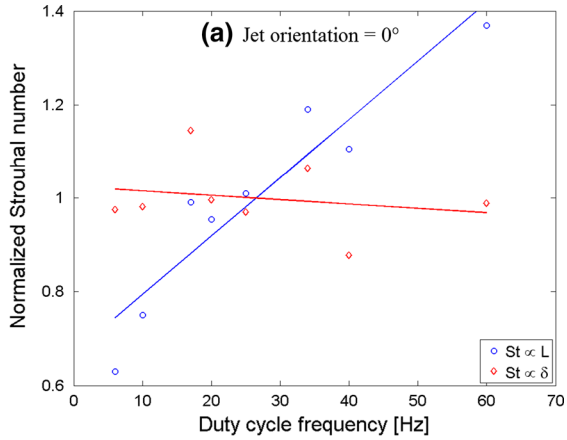

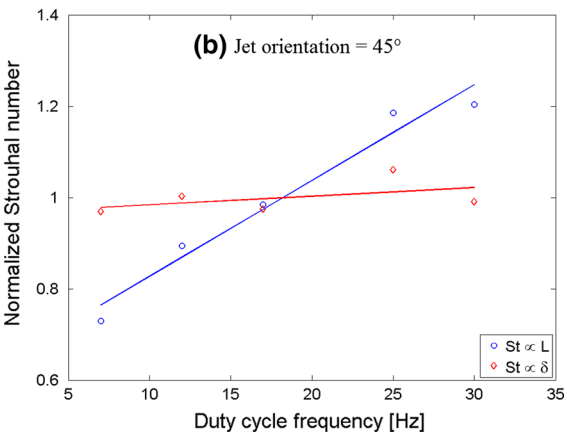

Fig. 12 Normalized Strouhal number as a function of the duty cycle frequency, with a jet orientation of 0° (**a**) and 45° (**b**)

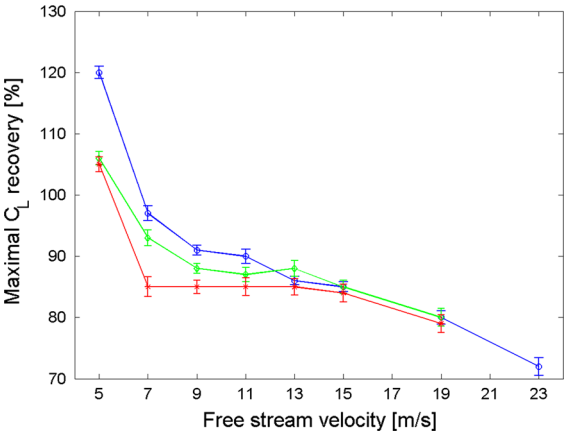

Fig. 13 Stall recovery C_L in percentage at the optimal duty cycle frequency as a function of the free stream velocity for an orientation of 0°, 45° and 90° of Jet 5

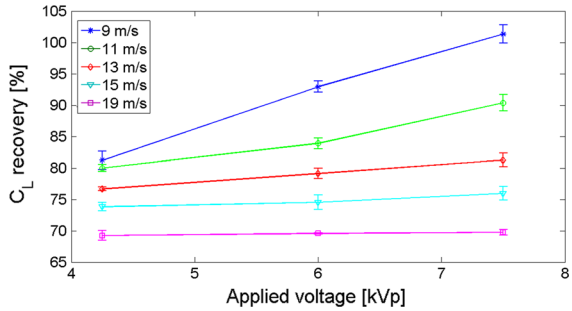

Fig. 14 Stall recovery in percentage as a function of the applied voltage obtained with the jet 5 at a 0° orientation, for free stream velocity in the range 9–19 m/s

the applied voltage. As reported by Neretti et al. [38], in still air and for the actuator operated in the continuous regime, the induced velocity linearly depends on the applied voltage. Thus the momentum transferred to the flow through the EHD effect increases with the applied voltage. As shown in Fig. 14 a similar behavior is observed with the actuator operated in the duty cycle regime.

5 Conclusions

In this paper the stall recovery obtained by means of a set of dielectric barrier discharge plasma actuators, on a standard NACA0015 airfoil in a wind tunnel flow, has been experimentally investigated. The actuators are designed to produce plasma jets with different directions (vectorized jets) and at different duty cycle frequencies (on/off cycles). The vectorized jets have been obtained by the interaction of two opposite jets produced tangentially to the actuator surface with different thrusts.

A first set of experiments has been carried out to evaluate the effect of the jet orientation on the stall recovery. The results show that the largest stall recovery effect comes from the jet closest to the leading edge of the airfoil. The orientation of the jet does not sensibly influence the stall recovery.

The recovery obtained by the duty cycle mode is more effective than that induced by the continuous operation of the DBD plasma actuator. In the duty cycle regime the Schlieren images of the flow show an operation of the DBD actuation similar to that of synthetic jets with the formation of vortices expanding in the direction of the induced flow.

In order to find the duty cycle frequency that maximize the stall recovery, Jet 5 has been operated with the orientations of 0° and 45°, and with several duty cycle frequencies. For this test an angle of attack of 26° and free stream velocities in the range between 5 and 23 m/s have been utilized. The optimal duty cycle frequency has been found to be a power law function of the free stream velocity with an exponent equal to 1.5, both for a jet orientations of 0° and of 45°. Therefore a relation between the duty cycle optimal frequency and the thickness of the boundary layer, taken as characteristic length for the determination of the Strouhal number, has been obtained.

An evaluation of the stall recovery obtained by Jet 5 with a direction of 0° at different supply voltages has been done with a free stream velocity in the range between 9 and 19 m/s and with a duty cycle frequency of 20 Hz. A linear relation between the increase of the stall recovery and the applied voltage has been observed. In this case, as in the continuous operation of the actuator, an increase of momentum transfer to the boundary layer flow due to the EHD effect, is observed when the applied voltage is increased.

The analysis has been performed in the open loop wind tunnel of the Applied Aerodynamic laboratory of the University of Bologna. The study has been accomplished without a velocity diagnostic, therefore no information on the actual state of the flow-field close to the element is provided, limiting a clear description of the underlying physics. Nonetheless, we believe that the results obtained may be of help for a better design and operating strategy of the control method.

Compliance with ethical standards

Conflict of interest The authors declare that they have no conflict of interest.

References

1. Neretti G (2016) Active flow control by using plasma actuators, recent progress in some aircraft technologies. In: Ramesh Agarwal (ed) InTech. doi: 10.5772/62720
2. Moreau E (2007) Airflow control by non-thermal plasma actuator. J Phys D Appl Phys 40:605. doi:10.1088/0022-3727/40/3/S01
3. Wang JJ, Choi K, Feng L, Jukes TN, Whalley RD (2013) Recent developments in DBD plasma flow control. Prog Aerosp Sci 62:52–78. doi:10.1016/j.paerosci.2013.05.003
4. Grundmann S, Tropea C (2007) Experimental transition delay using glow-discharge plasma actuators. Exp Fluids 42:653–657
5. Grundmann S, Tropea C (2008) Active cancellation of artificially introduced Tollmien–Schlichting waves using plasma actuators. Exp Fluids 44:795–806
6. Wilkinson SP (2003) Investigation of an oscillating surface plasma for turbulent drag reduction. In: Proceedings of the 41st aerospace sciences meeting and exhibit, Reno, USA, 2003. Paper AIAA 2003-1023
7. Touchard G (2008) Plasma actuators for aeronautical applications—state of art review. Int J Plasma Environ Sci Technol 2:1–25
8. Vernet J, Örlü R, Alfredsson PH (2015) Separation control by means of plasma actuation on a half cylinder approached by a turbulent boundary layer. J Wind Eng Ind Aerodyn 145:318–326
9. Greenblatt D, Ben-Harav A, Mueller-Vahl H (2014) Dynamic stall control on a vertical-axis wind turbine using plasma actuators. AIAA J 52(2):456–462
10. Borghi CA, Carraro MR, Cristofolini A, Neretti G (2008) Electrohydrodynamic interaction induced by a dielectric barrier discharge. J Appl Phys 103:063304. doi:10.1063/1.2888354
11. Borghi CA, Cristofolini A, Grandi G, Neretti G, Seri P (2015) A plasma aerodynamic actuator supplied by a multilevel generator operating with different voltage waveforms. Plasma Sour Sci Technol. doi:10.1088/0963-0252/24/4/045018
12. Pons J, Moreau E, Touchard G (2004) Electrical and aerodynamic characteristics of atmospheric pressure barrier discharges in ambient air. In: Proceedings of ISNTPT, pp 370–410
13. Opaits D, Likhanskii A, Neretti G, Zaidi S, Shneider M, Miles R, Macheret S (2008) Experimental investigation on dielectric barrier discharge plasma actuators driven by repetitive high-voltage nanosecond pulses with DC or low frequency sinusoidal bias. J Appl Phys 104:043304. doi:10.1063/1.2968251
14. Opaits D, Neretti G, Zaidi S, Shneider M, Miles R, Likhanskii A, Macheret S (2008) DBD plasma actuator driven by a combination of low frequency bias voltage and nanosecond pulses. In: 46th AIAA aerospace sciences meeting and exhibit, Reno Nevada, paper AIAA-2008-1372
15. Dawson R, Little J (2013) Characterization of nanosecond pulse driven dielectric barrier discharge plasma actuators for aerodynamic flow control. J Appl Phys 113:103302. doi:10.1063/1.4794507
16. Thomas FO, Corke TC, Iqbal M, Kozlov A, Schatzman D (2009) Optimization of dielectric barrier discharge plasma actuators for active aerodynamic flow control. AIAA J 47:2169–2178. doi:10.2514/1.41588
17. Cristofolini A, Neretti G, Roveda F, Borghi CA (2012) Schlieren imaging in a dielectric barrier discharge actuator for airflow control. J Appl Phys 111:033302. doi:10.1063/1.3682488
18. Cristofolini A, Borghi CA, Neretti G (2013) Charge distribution on the surface of a dielectric barrier discharge actuator for the fluid-dynamic control. J Appl Phys 113:143307. doi:10.1063/1.4799159
19. Cristofolini A, Neretti G, Borghi CA (2013) Effect of the charge surface distribution on the flow field induced by a

dielectric barrier discharge actuator. J Appl Phys 114:073303. doi:10.1063/1.4817378
20. Dragonas FA, Neretti G, Sanjeevikumar P, Grandi G (2015) High-voltage high-frequency arbitrary waveform multilevel generator for DBD plasma actuators. IEEE Trans Ind Appl. doi:10.1109/TIA.2015.2409262
21. Nishida H, Abe T (2011) Validation study of numerical simulation of discharge plasma on DBD plasma actuator. In: 42nd AIAA plasmadynamics and lasers conference. doi: 10.2514/6.2011-3913
22. Kotsonis M, Ghaemi S (2012) Performance improvement of plasma actuators using asymmetric high voltage waveforms. J Phys D Appl Phys 45(045204):12. doi:10.1088/0022-3727/45/4/045204
23. Neretti G, Cristofolini A, Borghi CA, Gurioli A, Pertile R (2012) Experimental results in DBD plasma actuators for air flow control. IEEE Trans Plasma Sci 40:1678–1687. doi:10.1109/TPS.2012.2191801
24. Post ML, Corke TC (2004) Separation control on high angle of attack airfoil using plasma actuators. AIAA J 42:2177–2184
25. He C, Corke TC, Patel MP (2009) Plasma flaps and slats: an application of weakly ionized plasma actuators. J Aircraft 46:864–873. doi:10.2514/1.38232
26. Rizzetta DP, Visbal MR (2011) Numerical investigation of plasma-based control for low-Reynolds-number airfoil flows. AIAA J 49:411–425. doi:10.2514/1.J050755
27. Bénard N, Moreau E (2014) Electrical and mechanical characteristics of surface AC dielectric barrier discharge plasma actuators applied to airflow control. J Exp Fluids 55:1846. doi:10.1007/s00348-014-1846-x
28. Bénard N, Jolibois J, Moreau E, Sosa R, Artana G, Touchard G (2008) Aerodynamic plasma actuators: a directional micro-jet device", 20th symposium on plasma science for materials (SPSM-20). J Thin Solid Films 516:6660–6667. doi:10.1016/j.tsf.2007.11.039
29. Amitay M, Glezer A (2002) Controlled transient of flow reattachment over stalled airfoils. Int J Heat Fluid Flow 23:690–699. doi:10.1016/S0142-727X(02)00165-0
30. Kim SH, Hong W, Kim C (2007) Separation control mechanism of airfoil using synthetic jet. J Mech Sci Technol 21:1367–1375
31. Santhanakrishnana A, Jacob J (2006) On plasma synthetic jet actuators. In: 44th AIAA aerospace science meeting and exhibit, reno, NV, paper AIAA 2006-317. doi 10.2514/6.2006-317
32. Bénard N, Jolibois J, Touchard G, Moreau E (2008) A directional plasma-jet device generated by double DBD actuators—an active vortex generator for aerodynamic flow control. In: 4th flow control conference, Seattle, Washington, paper AIAA 2008-3763
33. Bolitho M, Jacob J (2009) Active vortex generators using jet vectoring plasma actuators. SAE Int J Aerosp 1(1):610–618. doi:10.4271/2008-01-2234
34. Matsuno T, Kawaguchi M, Fujita N, Yamada G, Kawazoe H (2012) Jet vectoring and enhancement of flow control performance of trielectrode plasma actuator utilizing sliding discharge. In: 6th flow control conference, paper AIAA 2012-3238
35. Sosa R, Arnaud E, Memin E, Artana G (2009) Study of the flow induced by a sliding discharge. IEEE Trans Dielectr Electr Insul 16:305–311. doi:10.1109/TDEI.2009.4815157
36. Seney SD Jr, Huffman RE, Bailey W, Lui D, Reeder ME, Stults J (2011) Experimental study on the induced velocity of a three potential sliding discharge DBD actuator. In: 42nd AIAA plasma dynamics and laser conference, paper AIAA 2011-3732
37. Moreau E, Louste C, Touchard G (2008) Electric wind induced by sliding discharge in air at atmospheric pressure. J Electrostat 66:107–114. doi:10.1016/j.elstat.2007.08.011
38. Neretti G, Seri P, Taglioli M, Shaw A, Iza F, Borghi CA (2017) Geometry optimization of linear and annular plasma synthetic jet actuators. J Phys D Appl Phys. doi:10.1088/1361-6463/50/1/015210
39. Neretti G, Cristofolini A, Borghi CA (2014) Experimental investigation on a vectorized aerodynamic dielectric barrier discharge plasma actuator array. J Appl Phys 115:163304. doi:10.1063/1.4873896
40. Little J, Takashima K, Nishihara M, Adamovich I, Samimy M (2012) Separation control with nanosecond-pulse-driven dielectric barrier discharge plasma actuators. AIAA J 50(2):350–365
41. Post ML, Corke TC (2004) Separation control using plasma actuators–stationary and oscillating airfoils. In: AIAA paper 2004-0841
42. Thomas FO, Kozlov A, Corke TC (2008) Plasma actuators for cylinder flow control and noise reduction. AIAA J 46(8):1921–1931
43. Seifert A (2007) Closed-loop active flow control systems: actuators. In King R (ed) Active flow control: papers contributed to the conference "active flow control 2006"', Berlin, Germany, September 27–29. Springer, Berlin
44. Greenblatt D, Wygnanski IJ, Rumsey CL (2010) Aerodynamic flow control. In: John Wiley and Sons (eds) Encyclopedia of aerospace engineering. doi: 10.1002/9780470686652.eae019
45. Schlichting H, Kestin J (1960) Boundary layer theory, McGraw-Hill series in mechanical engineering. McGraw-Hill, New York